

0017-9310(95)00003-8

Heat transfer in the inverted meniscus type evaporator at high heat fluxes

D. KHRUSTALEV and A. FAGHRI

Department of Mechanical Engineering, University of Connecticut, Storrs, CT 06269-3139, U.S.A.†

(Received 22 July 1994 and in final form 7 November 1994)

Abstract—A one-dimensional mathematical model of the heat transfer during evaporation of the liquid from the liquid–vapor interface located in a porous structure into the dry region between the interface and the solid heated surface is developed for the case when the vapor flows through the narrow dry porous zone along the heated surface towards the vapor channel. The model predicts the location and shape of the liquid–vapor interface, the overall heat transfer coefficient, and the heat fluxes which can be recognized as critical for the evaporator. The numerical results are presented for the case of the miniature evaporator for electronic components cooling.

1. INTRODUCTION

Evaporators which are capable of withstanding high heat fluxes, for example larger than 100 W cm^{-2} , are of great interest for electronic components cooling systems. The most promising evaporator design is the so-called “inverted meniscus” type which has been considered by Raiff and Wayner [1], Feldman and Noreen [2] and Solov’ev and Kovalev [3]. These authors carried out some experimental and analytical investigations of the performance characteristics of the inverted meniscus type evaporators. However, some critical mechanisms related to the formation of the vapor blanket in the porous structure along the heated solid surface were not simulated numerically. In order to predict the critical heat flux and effective heat transfer coefficients in the evaporator, the following mathematical model has been developed. The model includes the following interconnected problems which are treated simultaneously in the frames of the numerical analysis.

- (1) Heat transfer during evaporation from a pore.
- (2) Heat transfer and vapor flow in the dry region of a porous structure with the stable side boundary, the location of which depends on the operational conditions.
- (3) Heat conduction in a solid fin (or wall) with a non-uniform heat sink on side surfaces.

These interconnected problems are considered in detail in the following sections.

2. PHYSICAL MODEL OF THE INVERTED MENISCUS EVAPORATOR

Schematics of the two configurations of the characteristic elements of the inverted meniscus evaporators

are shown in Fig. 1. In the first configuration (Figs. 1(a) and (b)), the heated triangular fin is inserted in the porous plate and sintered with it in order to provide good thermal contact. In the second configuration (Fig. 1(c)), the heated wall is flat. With a small heat flux, evaporation of the liquid, which saturates the porous element, can take place exclusively from the surface of the porous body into the vapor channel as shown in Fig. 1(a). However, with extremely high heat fluxes, which are significantly more interesting for the industrial applications, the existence of the stable vapor blanket inside the uniform porous structure along the heated solid surface was anticipated (Raiff and Wayner [1]; Solov’ev and Kovalev [3]; Wulz and Embacher [4]), as shown in Figs. 1(b) and (c). Note, that one more operational regime can possibly exist, which is unstable and referred to by Ku [5], where the vapor bubbles form at the heating surface and migrate until vented into the vapor channel. In the present paper only the case of the stable vapor blanket is considered. In this case evaporation takes place into the dry region of the porous structure at the liquid–vapor interface, the location of which shifts depending on the operational conditions. The heat is conducted to this interface from the heated surface through the dry region of the porous element, and the vapor flows mainly along the solid surface through this region towards the vapor channel. The vapor flow is provided by the capillary pressure gradient due to the difference in the curvature of the menisci along the liquid–vapor interface. While the vapor flow takes place in a comparatively narrow porous passage, the liquid with the same total mass flow rate (steady state) is filtered perpendicularly through the entire porous element to the liquid–vapor interface, and the pressure gradient in liquid along this interface is negligible in comparison to that in vapor. This assumption can be justified in the case

†This work was completed at Wright State University, Dayton, OH 45435, U.S.A.

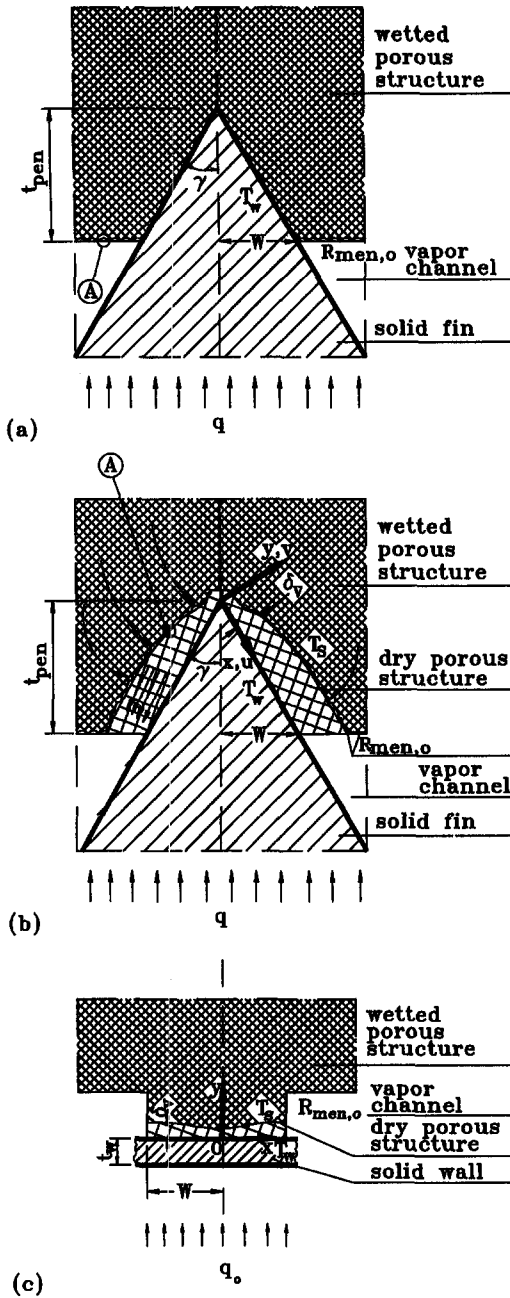


Fig. 1. Schematics of the modeled elements of the inverted meniscus evaporators: (a) with the triangular fin for low heat fluxes; (b) with the triangular fin for high heat fluxes and (c) with the flat heated wall for high heat fluxes.

the three parameters: the pressure in the liquid near the interface, $p_{l\delta}$, the temperature of the solid surface, T_0 , at $x = 0$, and the liquid–vapor meniscus radius at the end of the vapor blanket ($x = L_{v\delta}$), $R_{men,o}$. Note that the superheat of the fin exists at the following condition:

$$T_0 > T_{sat}(p_{l\delta} + 2\sigma/R_{men,min}) \quad (1)$$

where the subscript “sat” denotes the normal saturation temperature corresponding to a pressure

($p_{l\delta} + 2\sigma/R_{men,min}$) and $R_{men,min} = R_p/\cos\theta_{men,min}$. Inequality (1) characterizes the value of the solid–liquid superheat. $R_{men,o}$ is related to the fluid circulation in the entire device. For the case of the evaporator with the forced liquid supply it can be set $R_{men,o} \gg R_{men,min}$ because in this case the pressure drop in liquid is not due to the capillary pressure. For the case of the heat pipe, $R_{men,o}$ can be defined from the pressure balance for the whole heat pipe at the steady state

$$2\sigma/R_{men,o} = \Delta p_v + \Delta p_l + \Delta p_{p,l} \quad (2)$$

(provided that $R_{men,max} \rightarrow \infty$) where Δp_v is the pressure drop due to the vapor flow along the heat pipe, Δp_l is the pressure drop due to liquid flow along the liquid channels of the heat pipe, and $\Delta p_{p,l}$ is the pressure drop due to the liquid filtration through the porous plate in the evaporator section (and in the condenser section if it also contains the porous plate). That means that the capillary pressure drop presented in the left hand side of equation (2) supports the fluid circulation in the heat pipe while the capillary pressure drop $2\sigma(1/R_{men,min} - 1/R_{men,o})$ provides the vapor flow in the vapor blanket. Since these two pressure drops can be of the same order of magnitude, the existence of the vapor blanket in the inverted meniscus evaporator is important for the analysis of the heat pipe with evaporator of this type. At high heat fluxes the liquid–vapor interface doesn’t touch the solid superheated wall, $\delta_v|_{x=0} > 0$, and the liquid meniscus radius is supposed to reach its minimum, $R_{men,min}$, at least at one point along this interface. Note that analytical investigation by Solov’ev and Kovalev [3] was restricted by the case $\delta_v|_{x=0} = 0$. The vapor blanket thickness, δ_v , depends on the values of the mentioned parameters ($p_{l\delta}$, T_0 , and $R_{men,o}$), and can significantly affect the local effective evaporative heat transfer coefficient, h_{eff} . It can be anticipated that in the heat pipe with the considered evaporator an increase in the heat input causes a decrease of $R_{men,o}$ and the corresponding growth of the thickness of the dry zone. Therefore, the thermal resistance of the evaporator should increase with the heat flow rate in the heat pipe. This trend has been observed in the experiments by Solov’ev and Kovalev [3]. Note that the steady-state situation is modeled when no boiling of the liquid occurs at the liquid–vapor interface, and the phase change due to evaporation of the liquid at this interface takes place.

3. HEAT TRANSFER DURING EVAPORATION FROM A PORE

Evaporation of the liquid occurs from the surface of the liquid menisci situated at the liquid–vapor interface. Schematic of the cylindrical pore and liquid meniscus is shown in Fig. 2. The description of the heat transfer during evaporation from a pore is given here with the two following main assumptions.

- (1) The temperature of the solid–liquid interface T_s

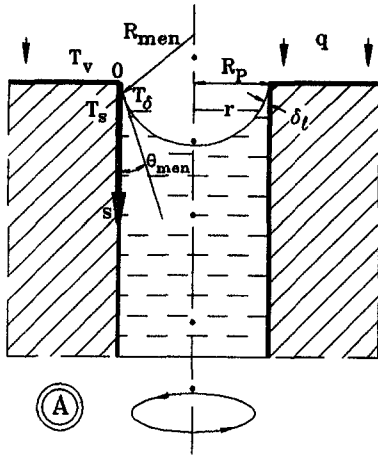


Fig. 2. Schematic of the evaporation from a cylindrical pore.

can be considered constant along the s coordinate for small s .

(2) The curvature of the axisymmetrical liquid-vapor surface of the meniscus is defined by the main radius of curvature $K = 2/R_{men}$ and hence is independent of s .

The validity of the second assumption has been proved numerically by Khrustalev and Faghri [6], where it was shown that this assumption could give an error less than 5% when calculating the overall heat transfer coefficient during evaporation from a capillary groove. Since heat transfer during evaporation from thin films in a pore is similar to that in a capillary groove, this assumption can be justified for the present analysis.

The local heat flux through the liquid film due to heat conduction is

$$q_1(s) = k_1 \frac{T_s - T_\delta}{\delta_1} \quad (3)$$

where the local thickness of the liquid layer δ_1 and the temperature of the free liquid film surface T_δ are functions of the s -coordinate. T_δ is affected by the disjoining and capillary pressures, and also depends on the value of the interfacial resistance, which is defined for the case of a comparatively small heat flux at the interface, q_δ , by the following relation given by the kinetic theory (Carey [7]):

$$q_\delta = - \left(\frac{2\alpha}{2-\alpha} \right) \frac{h_{fg}}{\sqrt{2\pi R_g}} \left[\frac{p_{v\delta}}{\sqrt{T_v}} - \frac{(p_{sat})_\delta}{\sqrt{T_\delta}} \right] \quad (4)$$

where $p_{v\delta}$ and $(p_{sat})_\delta$ are the saturation pressures corresponding to T_v and at the thin liquid film interface, respectively.

The relation between the saturation vapor pressure over the thin evaporating film, $(p_{sat})_\delta$, affected by the disjoining pressure, and the normal saturation pressure corresponding to T_δ , $p_{sat}(T_\delta)$, is given by the extended Kelvin equation (Carey [7]):

$$(p_{sat})_\delta = p_{sat}(T_\delta) \exp \left[\frac{(p_{sat})_\delta - p_{sat}(T_\delta) + p_d - \sigma K}{\rho_l R_g T_\delta} \right]. \quad (5)$$

Equation (5) reflects the fact that under the influence of the disjoining and capillary pressure, the liquid free surface saturation pressure $(p_{sat})_\delta$ is different from normal saturation pressure $p_{sat}(T_\delta)$ and varies along the thin film (or s -coordinate), while $p_{v\delta}$ and T_v are the same for any value of s . This is also due to the fact that T_δ changes along s . While the evaporating film thins approaching the point $s = 0$, the difference between $(p_{sat})_\delta$ given by equation (5) and the pressure obtained for a given T_δ using the saturation table becomes larger. This difference is the reason for the existence of the thin non-evaporating superheated film, which is in equilibrium state in spite of the fact that $T_\delta > T_v$.

Under steady state conditions, $q_1 = q_\delta$, and it follows from equations (3) and (4):

$$T_\delta = T_s + \frac{\delta_1}{k_1} \left(\frac{2\alpha}{2-\alpha} \right) \frac{h_{fg}}{\sqrt{2\pi R_g}} \left[\frac{p_{v\delta}}{\sqrt{T_v}} - \frac{(p_{sat})_\delta}{\sqrt{T_\delta}} \right]. \quad (6)$$

Equations (5) and (6) determine the interfacial temperature, T_δ , and pressure, $(p_{sat})_\delta$, for a given vapor pressure, $p_{v\delta}(x)$, temperature of the solid-liquid interface, T_s , and the liquid film thickness, $\delta_1(s)$.

As the liquid film thins, the disjoining pressure, p_d , and the interfacial temperature, T_δ , increase. Under specific conditions, a non-evaporating film thickness is present which gives the equality of the interfacial and solid surface temperatures, $T_\delta = T_s$. This is the thickness of the equilibrium non-evaporating film δ_0 . For water the following equation for the disjoining pressure was used in the present analysis (Holm and Goplen [8]):

$$p_d = \rho_l R_g T_\delta \ln \left[a \left(\frac{\delta_1}{3.3} \right)^b \right] \quad (7)$$

where $a = 1.5336$ and $b = 0.0243$. From equations (5)–(7), the following expression for the thickness of the equilibrium film is given:

$$\delta_0 = 3.3 \left\{ \frac{1}{a} \exp \left[\frac{p_{sat}(T_s) - p_{v\delta} \sqrt{T_s/T_v} + \sigma K}{\rho_l R_g T_s} \right] + \ln \left(\frac{p_{v\delta}}{p_{sat}(T_s)} \sqrt{\frac{T_s}{T_v}} \right) \right\}^{1/b}. \quad (8)$$

The total heat flow through a single pore is defined as

$$\begin{aligned} Q_p &= \int_0^{R_p} \frac{T_s - T_\delta}{\delta_1/k_1} 2\pi r \, ds \\ &\equiv \int_0^{R_p} \frac{T_s - T_\delta}{\delta_1/k_1} 2\pi R_{men} \\ &\quad \times \sin \left[\arctan \frac{R_p}{s + \sqrt{R_{men}^2 - R_p^2}} \right] ds. \quad (9) \end{aligned}$$

The surface of the pore wall is totally covered with microroughnesses, where the characteristic size varies from, for example, $R_r = 10^{-8}$ to 10^{-6} m. Apparently, the thin liquid film formation can be affected by some of these microroughnesses. The following approximation for the liquid film thickness was given by Khrustalev and Faghri [6]: for $\delta_0 \leq \delta_1 \leq \delta_0 + R_r$ and $R_r \gg \delta_0$

$$\delta_1 = \delta_0 + R_r - \sqrt{R_r^2 - s^2} - R_{\text{men}} + \sqrt{R_{\text{men}}^2 + s^2 + 2R_{\text{men}}s \sin \theta_f} \quad (10)$$

where for surface with microroughness $\theta_f = 0$, and the liquid film thickness in the interval $\delta_1 \geq \delta_0 + R_r$ is

$$\delta_1 = R_r + \delta_0 - R_{\text{men}} + (R_{\text{men}}^2 + s^2 + 2R_{\text{men}}s \sin \theta_{\text{men}})^{1/2}. \quad (11)$$

For the smooth surface model, θ_f is the angle between the solid-liquid and liquid-vapor interfaces at the point on s where the disjoining pressure and dK/ds become zero. Note that for small values of the accommodation coefficient (for example $\alpha = 0.05$) the value of R_r has not affected the total heat flow rate through the liquid film (Khrustalev and Faghri [6]).

The interfacial radius of curvature is related to the pressure difference between the liquid and vapor by the extended Laplace-Young equation:

$$p_{v\delta} - p_{l\delta} = \frac{2\sigma}{R_{\text{men}}} + \frac{\rho_v v_{v\delta}^2}{\varphi^2} \left(\frac{1}{\rho_l} - \frac{1}{\rho_v} \right) \quad (12)$$

where $v_{v\delta}$ is the vapor mean blowing velocity specified for a given meniscus, and φ is the porosity which is needed in this equation because the evaporation takes place into the dry region of the porous structure. Temperature of the saturated vapor near the interface, T_v , is related to its pressure by the saturation conditions:

$$T_v = T_{\text{sat}}(p_{v\delta}). \quad (13)$$

Then the heat transfer coefficient during evaporation from the porous surface is defined as

$$h_{e,p} = \frac{\varphi_s Q_p}{\pi R_p^2 (T_s - T_v)} \quad (14)$$

where $\varphi_s \equiv A_p/A_t$ is the surface porosity which is the ratio of the surface of the pores to the total surface of the porous structure for a given cross-section (in this paper it is assumed that $\varphi_s = \varphi$).

4. HEAT CONDUCTION IN THE SOLID FIN OR WALL

Since it can be anticipated that the temperature drops in metallic fin or wall are much smaller than those across the dry zone of the porous structure because $k_w \gg k_{\text{eff}}$, the heat conduction in the solid fin or wall is considered using a 1D approach. For the case of the flat wall (Fig. 1(c)) it means that dT_w/dy is not included in the consideration. The heat conduction in the triangular metallic fin is described by

the following equation (Fig. 1(b)), which was obtained as a result of energy balance on a differential element consideration:

$$\frac{d^2 T_w}{dx^2} + \frac{dT_w}{dx} \frac{1}{x} + (T_s - T_w) \frac{k_{\text{eff}} \cos \gamma}{x \delta_v(x) k_w \sin \gamma} = 0 \quad (15)$$

where T_s is the local temperature of the porous structure at the liquid-vapor interface location. Similarly, the heat conduction equation for the wall in Fig. 1(c) is

$$\frac{d^2 T_w}{dx^2} + (T_s - T_w) \frac{k_{\text{eff}}}{t_w \delta_v(x) k_w} + \frac{q_o}{t_w k_w} = 0. \quad (16)$$

The boundary conditions for equations (15) and (16) are

$$T_w|_{x=0} = T_0 \quad (17)$$

$$\left. \frac{dT_w}{dx} \right|_{x=0} = 0. \quad (18)$$

For the second configuration q_o is the uniform heat flux at the outer surface of the heated part of the flat wall. The value of q_o and the functions $\delta_v(x)$ and $T_s(x)$ should be given by the results of the vapor flow and heat transfer in the dry region solution considered below.

5. VAPOR FLOW AND HEAT TRANSFER IN THE DRY REGION OF THE POROUS STRUCTURE

The local heat flux due to heat conduction across the dry region of the porous structure from the solid surface to the liquid-vapor interface where evaporation takes place is

$$q_{\text{loc}}(x) = k_{\text{eff}} \frac{T_w(x) - T_s(x)}{\delta_v(x)}. \quad (19)$$

Equation (19) is valid for the case $k_v \ll k_{\text{eff}}$ and $c_{p,v}(T_w - T_s) \ll h_{fg}$. Hence, the mean velocity of the vapor flow for a given x along the solid surface is (the mass and energy conservation balances)

$$\begin{aligned} \bar{u}_v(x) &= \frac{1}{\delta_v(x) h_{fg} \rho_v} \int_0^x q_{\text{loc}}(x) dx \\ &\equiv \frac{k_{\text{eff}}}{\delta_v(x) h_{fg} \rho_v} \int_0^x \frac{T_w(x) - T_s(x)}{\delta_v(x)} dx \end{aligned} \quad (20)$$

where $\bar{u}_v(x)$ is the mean vapor velocity along the x -coordinate. The modified Darcy's equations for the vapor flow in both directions through a porous structure where the value of 0.55 is used for a dimensionless form-drag constant, Nield and Bejan [9], are

$$\frac{\partial p_v}{\partial x} = -\frac{\mu_v}{K} u_v(x) - \frac{0.55}{\sqrt{K}} \rho_v u_v^2(x) \quad (21)$$

$$\frac{\partial p_v}{\partial y} = \frac{\mu_v}{K} v_v(y) + \frac{0.55}{\sqrt{K}} \rho_v v_v^2(y) \quad (22)$$

where u_v and v_v are the area-averaged vapor velocities. The corresponding continuity equation is

$$\frac{\partial u_v}{\partial x} + \frac{\partial v_v}{\partial y} = 0. \quad (23)$$

It should be noted that the Darcy's equation is semi-empirical and describes the flow with the uniform velocity profile, therefore, it is assumed in the present analysis that u_v does not depend on y . Taking the definitions of the mean vapor pressure and axial velocity for a given x , \bar{p}_v and \bar{u}_v , into consideration (see the Nomenclature) and integrating equation (21) over y , the following equation can be obtained for the gradient of the mean vapor pressure along the x -coordinate

$$\frac{d\bar{p}_v}{dx} = -\frac{\mu_v}{K}\bar{u}_v(x) - \frac{0.55}{\sqrt{K}}\rho_v\bar{u}_v^2(x). \quad (24)$$

Since the situation when $\delta_v \ll L_{vb}$ is considered, the vapor pressure drop across the vapor blanket is much smaller than that along the x -coordinate. At the solid fin (or wall) surface $v_v|_{y=0} = 0$, and at the liquid-vapor interface $v_v|_{y=\delta_v} = v_{v\delta}\varepsilon$ where $\varepsilon = \cos[\arctan(d\delta_v/dx)]$ is the cosine of the angle between the y coordinate and the normal to the liquid-vapor interface and $v_{v\delta}$ is the blowing velocity (normal to the liquid-vapor interface):

$$v_{v\delta} = k_{\text{eff}} \frac{T_w - T_s}{\delta_v h_{fg} \rho_v}. \quad (25)$$

Equation (25) implies that the total amount of energy transferred from the heated solid surface to the liquid-vapor interface by the heat conduction across the dry porous zone, is spent on vaporization of the liquid. Since the axial velocity profile is nearly uniform, it follows from equation (23) that $v_v = v_{v\delta}\varepsilon y/\delta_v$. Integrating equation (22) twice over y for a given x and implementing the definition of \bar{p}_v , the difference between the vapor pressure near the liquid-vapor interface, $p_{v\delta}$, and the mean vapor pressure of the vapor flow, \bar{p}_v , for a given x can be estimated as follows

$$p_{v\delta} - \bar{p}_v = \delta_v \left(\frac{v_{v\delta}\varepsilon\mu_v}{3K} + \frac{0.55}{4\sqrt{K}}\rho_v v_{v\delta}^2 \varepsilon^2 \right). \quad (26)$$

Combining equations (20) and (24), finally we have for the vapor filtration flow pressure gradient along the x -coordinate:

$$\frac{d\bar{p}_v}{dx} = -\frac{v_v k_{\text{eff}}}{\delta_v h_{fg} K} \int_0^x \frac{T_w - T_s}{\delta_v} dx - \frac{0.55}{\rho_v \sqrt{K}} \left[\frac{k_{\text{eff}}}{\delta_v h_{fg}} \int_0^x \frac{T_w - T_s}{\delta_v} dx \right]^2 \quad (27)$$

The boundary condition for the equation (27) follows from equations (12), (25) and (26)

$$\bar{p}_v|_{x=0} = p_{l\delta} + \frac{2\sigma}{R_{\text{men}}|_{x=0}} + \frac{\rho_v^2 v_{v\delta}^2|_{x=0}}{\varphi^2} \left(\frac{1}{\rho_l} - \frac{1}{\rho_v} \right) - \frac{k_{\text{eff}}\mu_v\varepsilon(T_w - T_s)|_{x=0}}{3K h_{fg} \rho_v} - \frac{0.55\rho_v}{4\sqrt{K}} (\varepsilon^2 v_{v\delta}^2 \delta_v)|_{x=0}. \quad (28)$$

Now, the equation for T_s should be derived. The local heat flux at the liquid-vapor interface due to the evaporation of the liquid is:

$$q_{\text{loc}}(x) = [T_s(x) - T_v(x)]h_{e,p}(x). \quad (29)$$

Combining equations (19) and (29) because of the steady state situation in the consideration, the expression for the local temperature of the porous structure at the liquid-vapor interface location is:

$$T_s(x) = \frac{T_w(x) + h_{e,p}(x)T_v(x)\delta_v(x)/k_{\text{eff}}}{1 + h_{e,p}(x)\delta_v(x)/k_{\text{eff}}}. \quad (30)$$

Substituting equations (25) and (26) into equation (12) and differentiating it, the following equation for the radius of the meniscus curvature can be obtained

$$\begin{aligned} \frac{d}{dx} \left(\frac{2\sigma}{R_{\text{men}}} \right) &= \frac{d\bar{p}_v}{dx} - \frac{2\rho_v v_{v\delta}}{\varphi^2} \left(\frac{1}{\rho_l} - \frac{1}{\rho_v} \right) \\ &\times \frac{k_{\text{eff}}}{h_{fg}\delta_v^2} \left[\left(\frac{dT_w}{dx} - \frac{dT_s}{dx} \right) \delta_v - (T_w - T_s) \frac{d\delta_v}{dx} \right] \\ &+ \frac{k_{\text{eff}}\mu_v}{3K h_{fg} \rho_v} \left[\varepsilon \left(\frac{dT_w}{dx} - \frac{dT_s}{dx} \right) + (T_w - T_s) \frac{d\varepsilon}{dx} \right] \\ &+ \frac{0.55\rho_v}{4\sqrt{K}} \left(\frac{k_{\text{eff}}}{h_{fg}\rho_v\delta_v} \right)^2 \left\{ \varepsilon^2 \left[2(T_w - T_s) \left(\frac{dT_w}{dx} - \frac{dT_s}{dx} \right) \delta_v \right. \right. \\ &\left. \left. - (T_w - T_s)^2 \frac{d\delta_v}{dx} \right] + 2\varepsilon\delta_v(T_w - T_s)^2 \frac{d\varepsilon}{dx} \right\} \quad (31) \end{aligned}$$

with the boundary condition

$$R_{\text{men}}|_{x=0} = C_0 \quad (32)$$

where C_0 should be chosen from the constitutive condition for the minimum value of the meniscus radius along the liquid-vapor interface

$$\min \{ R_{\text{men}}(x) \} = R_p / \cos \theta_{\text{men},\text{min}}. \quad (33)$$

Now, the condition of the liquid-vapor interface mechanical equilibrium should be considered which is necessary in order to find its location or $\delta_v(x)$. In the analysis by Solov'ev and Kovalev [3] it was assumed that $\delta_v(x) = \text{const} \cdot x^{0.33}$ which is not quite satisfactory because of some reasons. For example, for the hypothetical situation when starting from a definite point along the x -coordinate, x_1 , there is no evaporation from the liquid-vapor interface, it should be $\delta_v|_{x>x_1} = \text{const}$, which condition is not satisfied by the discussed expression. Wulz and Embacher [4] have modeled the vapor flow in the uniform zone of the dry porous structure. The thickness of the vapor zone was determined as 0.1 mm at $q_{\text{max}} = 17500 \text{ W m}^{-2}$ by comparing the calculated temperature difference between the fin top and the phase boundary with the

value determined by experiment, using the simpler vapor zone model. Chung and Catton [10] have considered the problem of steam injection into a slow water flow through porous media, where the interface location was also unknown. They have found "... that the interface can be idealized as a stream line as far as the momentum equations are concerned." In the present paper the concept of a streamline is used indirectly as explained below. For the asymptotic case, $K \rightarrow \infty$, $\mu_v \rightarrow 0$, integrating Euler's equation along a streamline gives

$$p_v + \frac{\rho_v u_v^2}{2} + \frac{\rho_v v_v^2}{2} = p_v|_{x=0} \quad (34)$$

where the terms containing u_v^2 and v_v^2 correspond to the inertia effects due to acceleration of fluid. In the present analysis the vapor flow through a porous medium is described by Darcy's momentum equation. However, it is assumed that since the velocity profile of the vapor flow along the x -coordinate, u_v , is nearly uniform, equation (34) can be used for the description of the inertia effects at the liquid-vapor interface concerning acceleration of the vapor. It can be anticipated that the liquid-vapor interface can be stable provided it has the shape which eliminates the influence of the inertia effects due to acceleration of the vapor flow on the vapor pressure near this interface. While the steady-state situation is analyzed, the liquid pressure along the interface is constant, and the pressure losses in the vapor flow in both directions due to friction and solid obstacles are compensated by the capillary pressure, the vapor pressure gradient along the stable interface due to these inertia effects should be equal to zero. Since the velocity profile of the vapor flow along the x -coordinate is nearly uniform, it follows from equation (34)

$$\frac{\rho_v \bar{u}_v^2}{2} + \frac{\rho_v v_{v\delta}^2 \varepsilon^2}{2} = \text{const.} \quad (35)$$

Note that equation (35) is not used for the fluid flow in the porous medium but describes the inertia effects at the adjustable liquid-vapor interface while the momentum equations for the vapor flow in the porous medium are concerned. Equation (35) is necessary in order to find the equilibrium location of the liquid-vapor boundary. Substituting equation (20) and (25) into equation (35) and differentiating it after some rearrangements gives the equation for the vapor blanket thickness, δ_v :

$$\begin{aligned} \frac{d^2 \delta_v}{dx^2} \left\{ \delta_v (T_w - T_s)^2 \varepsilon \sin \left(\arctan \frac{d\delta_v}{dx} \right) \left[1 + \left(\frac{d\delta_v}{dx} \right)^2 \right]^{-1} \right\} \\ = (T_w - T_s) \left[\int_0^x \frac{T_w - T_s}{\delta_v} dx + \delta_v \varepsilon^2 \left(\frac{dT_w}{dx} - \frac{dT_s}{dx} \right) \right] \\ - \frac{d\delta_v}{dx} \left[\left(\int_0^x \frac{T_w - T_s}{\delta_v} dx \right)^2 + \varepsilon^2 (T_w - T_s)^2 \right] \quad (36) \end{aligned}$$

where all of the terms containing $(T_w - T_s)$ can be

calculated in the numerical procedure using the functions $T_w(x)$ and $T_s(x)$ determined at the previous iteration. The second-order differential equation (36) should be solved with the two boundary conditions for the variables δ_v and $d\delta_v/dx$. The first boundary condition is

$$\delta_v|_{x=0} = C_1. \quad (37)$$

C_1 should be chosen from the constitutive condition that it is the value of $\delta_v|_{x=0}$ which provides the satisfaction of the following boundary condition

$$R_{\text{men}}|_{x=L_{vb}} = R_{\text{men},o}. \quad (38)$$

The second boundary condition is due to the symmetry of the considered element (Fig. 1). Since at the point $x = 0$ $dT_w/dx = 0$, $dT_s/dx = 0$, and $dv_{v\delta}/dx = 0$ because of the physical reasons, it follows from equation (25)

$$\frac{d\delta_v}{dx} \Big|_{x=0} = 0. \quad (39)$$

Thus we have six main variables (or unknown functions $f_i(x)$): $p_{v\delta}$, \bar{p}_v , R_{men} , T_s , $v_{v\delta}$ and δ_v which should be found from the six equations: (12), (25), (27), (30), (31) and (36). These six equations should be solved along with those presented in the previous sections for variables $h_{e,p}(x)$ and $T_w(x)$. Note that the value q_o which is needed for equation (16) now can be found as:

$$q_o = \frac{1}{W} \int_0^{L_{vb}} k_{\text{eff}} \frac{T_w(x) - T_s(x)}{\delta_v(x)} dx. \quad (40)$$

For the first configuration, q_o is the heat flux in the solid fin corresponding to the porous structure-vapor channel plane. The heat flux on the outer surface of the evaporator (and the corresponding effective heat transfer coefficient) can be recalculated taking the geometry of the evaporator into consideration. Although the vapor leaving the dry zone of the porous structure is superheated, it is convenient to relate the local effective heat transfer coefficient to the vapor saturation temperature because $c_{p,v}(T_w - T_s) \ll h_{fg}$. Thus the local effective heat transfer coefficient corresponding to the point $x = L_{vb}$ (outlet of the vapor flow) is defined as:

$$h_{\text{eff}} = \frac{1}{W(T_w - T_v)_o} \int_0^{L_{vb}} k_{\text{eff}} \frac{T_w(x) - T_s(x)}{\delta_v(x)} dx. \quad (41)$$

6. NUMERICAL TREATMENT

The numerical procedure was organized as a sequence of the steps:

(1) the initial approximation for the functions $\delta_v(x)$, $h_{e,p}$, $T_w(x)$ and $R_{\text{men}}(x)$ was chosen: $\delta_v(x) = C_1 + C_2x$, $T_w(x) = T_0$, $R_{\text{men}}(x) = R_{\text{men},\text{min}}$ ($C_0 + C_3x/t_{\text{pen}}$) and $h_{e,p} = C_4$;

(2) the function $p_{v\delta}(x)$ (actually $p_{v\delta}(x) - p_{l\delta}$) was calculated from equation (12) with $v_{v\delta} = C_5$;

(3) the function $T_v(x)$ was calculated from the saturation table;

(4) the function $T_s(x)$ was calculated from equation (30);

(5) the function $v_{v\delta}(x)$ was calculated from equation (25);

(6) equations (27), (31) and (36) with the boundary conditions (28), (32), (37) and (39) were solved using the Runge–Kutta procedure and new functions $\bar{p}'_v(x)$, $1/R'_{men}(x)$ and $\delta'_v(x)$ were found;

(7) equation (15) (or equation (16) for the second configuration) with the boundary conditions (17) and (18) was solved for the variables T_w and dT_w/dx using the Runge–Kutta procedure and new function $T'_w(x)$ was obtained;

(8) new functions $p'_{v\delta}$ and $T'_v(x)$ were calculated from equation (12) and the saturation table;

(9) equations (5)–(13) were solved for every point on x and new function $h'_{e,p}(x)$ was found;

(10) the values of q_o (equation (40)) and h_{eff} (equation (41)) were calculated;

(11) every previous function, f_i , was replaced by the new one using new function, f'_i , according to the following formula:

$$f_i(x) + \Delta_i [f_i(x)' - f_i(x)] \rightarrow f_i(x)$$

where Δ_i belong to the interval from zero to unity; and steps (4)–(10) were repeated many times until the convergence of the solution has been reached (about 90–150 iterations were required to gain the converged solution for every of the functions: $\max\{|f'_i - f_i|/f_i\} \leq 0.001$) and

(12) the smaller value of C'_1 was set and the steps (1)–(11) were repeated several times with different C_1 until the boundary condition $R_{men}|_{x=L_{vb}} = R_{men,o}$ has been satisfied.

The results were obtained with constant thermophysical properties corresponding to the saturation temperature $T_{sat}(p_{l\delta}) = 100^\circ\text{C}$.

7. RESULTS AND DISCUSSION

In order to verify the assumption that the liquid pressure along the liquid–vapor interface, $p_{l\delta}$, can be considered constant, the following estimation for the pressure drop in the wetted porous structure was made for all of the numerical results with the calculated values of q_o :

$$\Delta p_{pen,l} = \frac{t_{pen}\mu_l}{K} \frac{q_o}{h_{fg}\rho_l} \quad (42)$$

and $\Delta p_{pen,l}$ values were compared with the calculated pressure drops in the vapor blanket along the fin surface, $\Delta p_{pen,v} = \bar{p}_v|_{x=0} - \bar{p}_v|_{x=L_{vb}}$. For the presented numerical results the values of the $(\Delta p_{pen,l}/\Delta p_{pen,v})$ were less than 0.5% which proves the validity of the accepted assumption. This also means that solving the corresponding 2D problem for the liquid pressure in

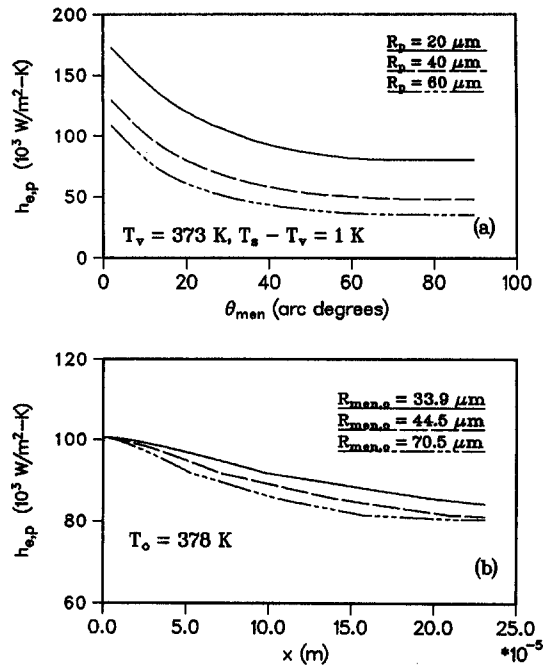


Fig. 3. Heat transfer coefficient during evaporation from the porous surface: (a) vs liquid meniscus contact angle (for a single pore) and (b) along the heated fin surface.

the wetted porous structure (Cao and Faghri [11]) simultaneously with the problem solved in the present paper would not cause significant changes in the presented numerical results. In that case the pressure in liquid along the liquid–vapor interface would be a comparatively weak function of x , $p_{l\delta}(x)$, which would result in only a slightly different menisci radii distribution along the x -coordinate, $R_{men}(x)$, because the vapor pressure distribution in the dry zone of the porous structure, $\bar{p}_v(x)$, is the predominant function for the considered situation.

The numerical results were obtained for the first configuration (Fig. 1(b)) for the case of the miniature evaporator: $\gamma = 30^\circ$, $t_{pen} = 0.2$ mm, $R_p = 20$ μm , $R_r = 0.02$ μm , $\theta_{men,min} = 33^\circ$ (Stepanov *et al.* [12]), $\alpha = 0.05$ (Paul [13]), $k_{eff} = 10$ $\text{W m}^{-1} \text{K}^{-1}$, $k_w = 438$ $\text{W m}^{-1} \text{K}^{-1}$, $\phi = 0.5$, $\phi_s = 0.5$, $K = 0.5 \times 10^{-12}$ m^2 , $p_{l\delta} = 1.013 \times 10^5$ Pa, and the working fluid was water.

Since the longitudinal circulation of the fluid in the heat pipe which determines the value of $R_{men,o}$ was not considered in the present analysis, the numerical results were obtained for several fixed values of $R_{men,o}$.

The maximum values of Reynolds numbers for the vapor flow in the dry zone, $Re_v = \bar{u}_v \sqrt{K}/\nu_v$, in the numerical experiments were up to 250, which means that the quadratic term in the modified Darcy's equation was predominant. Moreover, the vapor flow in the pores at high heat fluxes could be turbulent. Note that for the turbulent regime the macroscopic equations (21), (22) and (24) are still applicable (Nield and Bejan [9]).

The data in Fig. 3 show that the heat transfer

coefficient during evaporation from the porous surface, $h_{e,p}$, significantly depended on the curvature of the liquid meniscus (Fig. 3(a)) and, hence, changed along the liquid vapor interface (Fig. 3(b)) because the curvature of the liquid menisci changed along this interface. For smaller pore sizes the values of $h_{e,p}$ are larger because of the larger relative surface occupied by the thin films.

The thickness of the dry zone increased along the x -coordinate as shown in Fig. 4(a), and the value of $C_1 \equiv \delta_v|_{x=0}$ increased as $R_{men,o}$ decreased for a given superheat value, $T_0 - T_v|_{x=0}$. For the larger values of $\delta_v|_{x=0}$ variation of the vapor blanket thickness along the x -coordinate becomes weaker. The liquid menisci radii changed along the liquid-vapor interface so that the capillary pressure gradient provided the vapor flow in both directions in the dry zone, Fig. 4(b). The average vapor pressure drop along the x -coordinate reached several thousand Pascals, Fig. 4(c). The minimum physically reasonable average pressure in the vapor blanket, $\bar{p}_v \rightarrow p_{1\delta}$, can occur in the situation

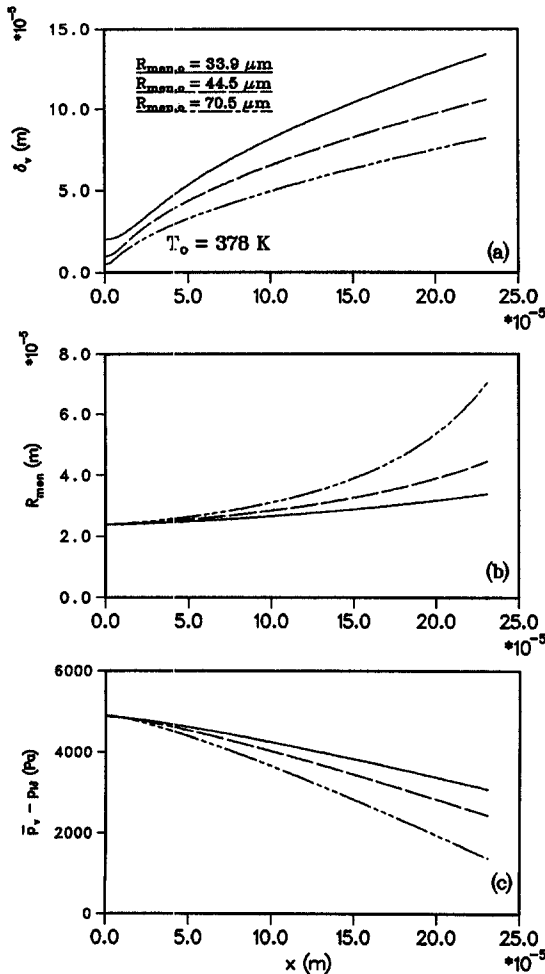


Fig. 4. Performance characteristics of the modeled evaporator element along the heated fin surface : (a) vapor blanket thickness ; (b) liquid menisci radii and (c) mean vapor-liquid pressure drop.

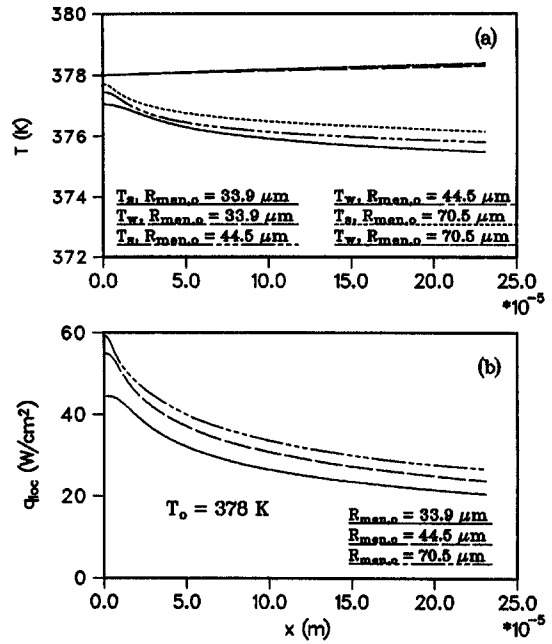


Fig. 5. Performance characteristics of the modeled evaporator element along the heated fin surface : (a) temperatures of the fin surface and of the porous structure at the liquid-vapor interface and (b) local heat flux across the vapor blanket.

when the liquid-vapor meniscus radius is still greater than zero. The temperature drops at the solid heated surface were significantly smaller than those corresponding to the porous skeleton at the liquid-vapor interface, Fig. 5(a). The real superheat of the liquid, $T_s - T_v$, which could initiate the boiling, was significantly smaller than the superheat of the heated solid surface: $T_s - T_v < T_w - T_v$. The local heat fluxes across the dry zone had their maximums at the point $x = 0$, Fig. 5(c).

The data presented in Fig. 6 were obtained for the case $R_{men,o} > 8R_{men,min}$ which corresponds to the evaporator with the forced liquid supply. The thickness of the dry zone at the point $x = 0$, C_1 , and the superheat of the solid surface at the point $x = L_{vb}$, which is the outlet of the vapor flow, $(T_w - T_v)_o$, increased progressively with the heat flux, q_o , while the effective heat transfer coefficient, h_{eff} , decreased as shown in Fig. 6. In the situation when the minimum thickness of the porous element could be $100 \mu\text{m}$, at the heat flux of $q_o = 200 \text{ W cm}^{-2}$ while $C_1 = 100 \mu\text{m}$, the dry out of the evaporator could occur due to the penetration of the vapor into the liquid channels. If the temperature drop on the evaporator was restricted by 20 K because of the technical reasons, the maximum corresponding heat flux could be no more than $q_o = 200 \text{ W cm}^{-2}$. For the case of the heat pipe with a heat load corresponding to the heat fluxes in consideration, the value of $R_{men,o}$ would be significantly smaller than $8R_{men,min}$ which could result in the larger thickness of the dry zone for the same q_o . The increase of the permeability of the porous structure resulted in

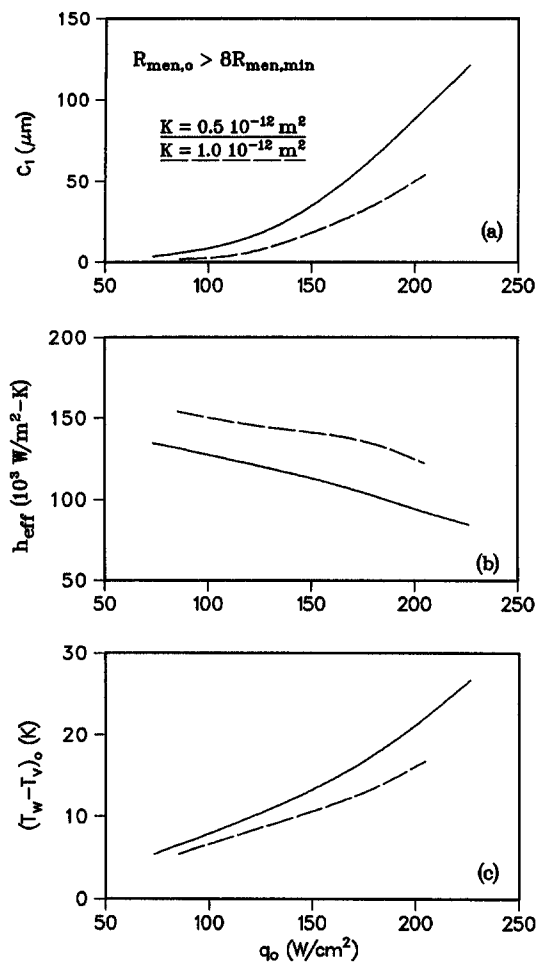


Fig. 6. Influence of the heat flux on the performance characteristics of the modeled element ; (a) vapor blanket thickness at $x = 0$; (b) effective heat transfer coefficient and (c) the superheat of the fin surface.

the decrease of the thickness of the vapor blanket for the same operational conditions and, hence, could provide higher critical heat fluxes.

For extremely high heat fluxes, q_{loc} , when the temperature drop ($T_s - T_v$) is large, boiling of the liquid at the liquid-vapor interface can occur which can cause instabilities at the liquid-vapor interface. However, boiling of the liquid does not necessarily result in the dry out of the evaporator of this type. Since $q_0 > q_{loc}$ due to $L_{vb} > W$, the triangular geometry of the solid fin helps to postpone boiling and, therefore, can be advantageous compared to the case of the flat wall in the second configuration shown in Fig. 1(c). In other words, the triangular geometry of the fin provides higher value of the heat flux on the outer surface of the evaporator which corresponds to the beginning of the boiling of the liquid at the liquid-vapor interface.

8. CONCLUSIONS

(1) The numerical results proved the possibility of the existence of the stable dry zone (vapor blanket) in

the porous structure along the heated solid surface for a definite interval of the heat fluxes.

(2) The pressure drop in the vapor blanket along the fin surface with the turbulent vapor flow in the pores was many times larger than the estimated pressure drop in liquid over the porous element which enabled to assume the liquid pressure to be constant along the liquid-vapor boundary.

(3) Two critical mechanisms were observed in the inverted meniscus evaporator, both being related to the increase of the vapor blanket in the porous plate for increasing heat fluxes. The first mechanism was the growth of the evaporator thermal resistance for increasing heat fluxes which could lead to an unacceptable thermal resistance of the evaporator in the case when the thermal conductivity of the porous structure was low. The second mechanism was the dry out of the evaporator which could take place for a definite heat flux q_{max} in the situation when the vapor blanket thickness at the fin top was equal to the minimum thickness of the porous plate. Thus, for the case of a heat pipe, the dry out of the inverted meniscus type evaporator can occur before the traditional capillary limit or the conditions for the beginning of the boiling are reached.

Acknowledgements—Funding for this work was provided by a joint effort of the SDI and Thermal Energy Group of the Aero Propulsion Laboratory of the U.S. Air Force under contract no. F33615-92-C-2276.

REFERENCES

1. R. J. Raiff and P. C. Wayner, Jr., Evaporation from a porous flow control element on a porous heat source, *Int. J. Heat Mass Transfer* **16**, 1919–1929 (1973).
2. K. T. Feldman and D. L. Noreen, Design of heat pipe cooled laser mirrors with an inverted meniscus evaporator wick, AIAA paper 92-0148 (1980).
3. S. L. Solov'ev and S. A. Kovalev, Heat transfer and hydrodynamics in the inverted meniscus evaporator of a heat pipe, *Proceedings of the Sixth International Heat Pipe Conference*, Grenoble, France, Vol. I, pp. 116–120 (1987).
4. H. Wulz, and E. Embacher, Capillary pumped loops for space applications experimental and theoretical studies on the performance of capillary evaporator designs, *Proceedings of the AIAA/ASME Fifth Joint Thermophysics and Heat Transfer Conference*, Seattle, WA, AIAA paper 90-1739 (1990).
5. J. Ku, Overview of capillary pumped loop technology, *Proceedings of the Twenty Ninth National Heat Transfer Conference*, Atlanta, GA (1993).
6. D. Khrustalev and A. Faghri, Heat transfer during evaporation and condensation on capillary-grooved structures of heat pipes, *Proceedings of the 1994 International Mechanical Engineering Congress*, Chicago, IL (1994).
7. V. P. Carey, *Liquid-Vapor Phase-Change Phenomena: An Introduction to the Thermophysics of Vaporization and Condensation Processes in Heat Transfer Equipment*, p. 117. Hemisphere, New York (1992).
8. F. W. Holm and S. P. Gopen, Heat transfer in the meniscus thin-film transition region, *ASME J. Heat Transfer* **101** (3), 543–547 (1979).

9. D. A. Nield and A. Bejan, *Convection in Porous Media*, p. 9. Springer, New York (1992).
10. M. Chung and I. Catton, Steam injection into a slow water flow through porous media, *ASME J. Heat Transfer* **115**, 734–743 (1993).
11. Y. Cao and A. Faghri, Conjugate analysis of a flat-plate type evaporator for capillary pumped loops with three-dimensional vapor flow in the groove, *Int. J. Heat Mass Transfer* **37** (3), 401–409 (1994).
12. V. G. Stepanov, L. D. Volyak and Yu. V. Tarlakov, Wetting contact angles for some systems, *J. Engng Physics Thermophys.* **32** (6), 1000–1003 (1977).
13. B. Paul, Compilation of evaporation coefficients, *ARS J.* **32**, 1321–1328 (1962).